Molecular Therapy
Nucleic Acids
Original Article

Selection of a novel cell-internalizing RNA aptamer specific for CD22 antigen in B cell acute lymphoblastic leukemia

Dario Ruiz-Ciancio,[1,2] Li-Hsien Lin,[3] Suresh Veeramani,[3,4] Maya N. Barros,[3] Diego Sanchez,[5] Ary Lautaro Di Bartolo,[6] Diego Masone,[6] Paloma H. Giangrande,[3,7] María Belén Mestre,[1,2] and William H. Thiel[3]

[1]Instituto de Ciencias Biomédicas (ICBM), Facultad de Ciencias Médicas, Universidad Católica de Cuyo, Av. José Ignacio de la Roza 1516, Rivadavia, San Juan 5400, Argentina; [2]National Council of Scientific and Technical Research (CONICET), Godoy Cruz 2290, Ciudad Autónoma de Buenos Aires C1425FQB, Argentina; [3]Department of Internal Medicine, University of Iowa, Iowa City, IA 52246, USA; [4]Holden Comprehensive Cancer Center, University of Iowa, Iowa City, IA 52242, USA; [5]Instituto de Medicina y Biología Experimental de Cuyo (IMBECU), CONICET, CCT-Mendoza 5500, Argentina; [6]Instituto de Histología y Embriología de Mendoza (IHEM) – Consejo Nacional de Investigaciones Científicas y Técnicas (CONICET), Universidad Nacional de Cuyo (UNCuyo), Mendoza M5502JMA, Argentina; [7]VP Platform Discovery Sciences, Biology, Wave Life Sciences, 733 Concord Avenue, Cambridge, MA 02138, USA

Despite improvements in B cell acute lymphoblastic leukemia (B-ALL) treatment, a significant number of patients experience relapse of the disease, resulting in poor prognosis and high mortality. One of the drawbacks of current B-ALL treatments is the high toxicity associated with the non-specificity of chemotherapeutic drugs. Targeted therapy is an appealing strategy to treat B-ALL to mitigate these toxic off-target effects. One such target is the B cell surface protein CD22. The restricted expression of CD22 on the B-cell lineage and its ligand-induced internalizing properties make it an attractive target in cases of B cell malignancies. To target B-ALL and the CD22 protein, we performed cell internalization SELEX (Systematic Evolution of Ligands by EXponential enrichment) followed by molecular docking to identify internalizing aptamers specific for B-ALL cells that bind the CD22 cell-surface receptor. We identified two RNA aptamers, B-ALL1 and B-ALL2, that target human malignant B cells, with B-ALL1 the first documented RNA aptamer interacting with the CD22 antigen. These B-ALL-specific aptamers represent an important first step toward developing novel targeted therapies for B cell malignancy treatments.

INTRODUCTION

Cancer is a major cause of death of children worldwide,[1] with acute lymphoblastic leukemia (ALL) the most frequent cancer in pediatric oncology among children below the age of 19.[2,3] ALL is a malignant disorder characterized by clonal proliferation of early B and T lymphocyte precursor cells, with B cell leukemia (B-ALL) accounting for around 80% of ALL pediatric cases.[4] Conventional treatment options for patients with B-ALL have improved in the last decade, with long-term survival at 60%–80% for children and 25%–35% for adults.[1,5] Unfortunately, patients with recurring disease encounter challenges associated with chemotherapy cytotoxicity and high mortality. These challenges indicate that there is still a significant need for development of novel targeted therapies for B-ALL.

Numerous antigen-based therapies have been proven to be efficacious in relapsed or refractory B-ALL.[6,7] The cell-surface protein cluster of differentiation 22 (CD22) has arisen as an important B-ALL therapeutic antigen. CD22 is expressed in the majority of tumoral B lymphoblastic cells and internalizes upon ligand binding through a constitutive clathrin-mediated endocytosis process that permits targeted delivery of immunotoxins into the cytoplasm of B cells.[8–10] Two anti-CD22-drug-conjugated antibodies, inotuzumab ozogamicin[11] and moxetumomab pasudotox,[12] have been approved recently by the US Food and Drug Administration (FDA) for B cell malignancies. Additional anti-CD22 monoclonal antibody-based therapies are currently under development, including epratuzumab[13] and an anti-CD22 chimeric antigen receptor T (CAR-T) cell.[14–16] Antibody-drug conjugate (ADC) and CAR-T cells have produced dramatic advances in hematologic cancer treatment, but challenges remain.[17] ADC still faces obstacles that include high costs, off-target toxicities, and increased clearance rates.[18] In addition, ADC therapies for B-ALL have shown limited success, primarily because of limited tumor penetration, acquired resistance, and unknown benefits in combination with other cancer therapies.[19] Barriers to effective CAR-T cell therapy include severe life-threatening toxicities such as cytokine release syndrome, primary resistance to CAR-T cells, and response followed by relapse post CAR-T cell treatment. Current

Received 28 November 2022; accepted 25 July 2023;
https://doi.org/10.1016/j.omtn.2023.07.028.

Correspondence: William H. Thiel, Department of Internal Medicine, University of Iowa, Iowa City, IA 52246, USA.
E-mail: william-thiel@uiowa.edu
Correspondence: María Belén Mestre, Instituto de Ciencias Biomédicas (ICBM), Facultad de Ciencias Médicas, Universidad Católica de Cuyo, Av. José Ignacio de la Roza 1516, Rivadavia, San Juan 5400, Argentina.
E-mail: bmestreg@gmail.com
Correspondence: Paloma H. Giangrande, Department of Internal Medicine, University of Iowa, Iowa City, IA 52246, USA.
E-mail: pgiangrande@wavelifesci.com

challenges will likely be surmounted by development of novel agents that improve existing targeted approaches.

Aptamers have emerged as promising reagents for diagnostic and therapeutic applications.[20,21] Aptamers are short (25–100 nt), synthetic, single-stranded DNA or RNA molecules that fold into complex tertiary structures that allow an aptamer to bind a target molecule or cell type with high affinity and specificity.[20–22] Similar to antibodies, aptamers are capable of binding to a specific target molecule with high accuracy. They may, for example, distinguish between conformational isomers[23] or identify single point mutations.[24] In terms of affinity, aptamers and antibodies showed high-affinity binding interactions with their targets at nano- to picomolar levels.[22,25] However, unlike antibodies, aptamers have been found to cause low or no immunogenicity in standard assays, although some differences may arise between different individual aptamer sequences.[26,27] Adverse toxicity data regarding aptamer use in clinical trials are limited, with only one recorded incidence of an elicited immune response following administration, but data suggest that the response was to the conjugated polyethylene glycol (PEG) of the PEGylated aptamer REG1.[28,29] Although aptamers have better tissue penetration than antibodies because of their smaller size (8–15 kDa for aptamers versus 150 kDa for antibodies), it makes aptamers susceptible to kidney filtration and a short circulation time *in vivo*.[30] Therefore, aptamers can be chemically synthesized with additional modifications (e.g., PEGylation, biotin, fluorophores, small interfering RNAs [siRNAs]) to improve their pharmacokinetic profile and prolong half-life.[31–34] Despite great progress having been made in research of aptamers for oncology applications, clinical translation of aptamers is still very limited, with only one FDA-approved aptamer-based drug available to date.[35] Nevertheless, various promising aptamer-based probes for cancer diagnosis and therapy are currently being tested in clinical trials with encouraging results.[36,37]

Aptamers are identified through a process called SELEX (systematic evolution of ligands by exponential enrichment).[38,39] The SELEX process was first introduced by Tuerk et al.[40] and Ellington and Szostak[41] in the early 1990s to isolate high-affinity ligands from a combinatorial single-stranded nucleic acid library using repeated rounds of positive and negative selection pressure. The initial aptamer library usually comprises a collection of 10^{14}–10^{15} different aptamer sequences, depending on the length of the variable region, which provides up to 4^N sequence diversity (with N defined as the length of the variable region).[42] The cell internalization SELEX process has modified SELEX to identify aptamers that bind and gain entry into specific cell types.[39,43,44] These cell-internalizing aptamers have been used successfully as a platform to deliver therapeutics, such as cytotoxic siRNAs, specifically into cancer cells.[45–47] Here, we describe application of cell internalization SELEX to identify RNA aptamers that specifically target and internalize into B-ALL cells. From these B-ALL-specific aptamers, we identified the first reported RNA aptamer that targets CD22, an important internalizing cell-surface receptor expressed by B-ALL cells. These B-ALL-targeting RNA aptamers represent an important first step toward development of therapeutics that can target B cell malignancies.

RESULTS

B-ALL cell internalization SELEX

To enrich for aptamers that selectively internalize into B-ALL cells, the cell internalization SELEX protocol that is typically used with adherent cells was adapted and optimized for cells grown in suspension (Figure 1).[22,38,43] For positive selection pressure, the B-ALL cell internalization SELEX protocol utilized two B-ALL cell lines: the pre-B-ALL cell line NALM-16 and the common B-ALL cell line KOPN-8. Pre-B-ALL and common B-ALL account for 90%–95% of ALL.[48] Therefore, using the NALM-16 and KOPN-8 cell lines during SELEX should enrich for aptamers that interact with cell-surface proteins expressed by most types of B-ALL cancers. For negative selection pressure, three cell types were used: the T cell ALL (T-ALL) line Jurkat, the human endothelial cell line Ea.Hy926, and human peripheral white blood cells (hWBC) collected from healthy individuals. Jurkat cells were introduced to eliminate aptamers that interact with proteins common to B- and T-ALL cells, whereas Ea.Hy926 cells and hWBCs were introduced to mitigate interaction with human vasculature and immune cells. To achieve greater reproducibility in the earlier rounds of selection, hWBCs were not applied until round 9 because of their highly variable composition compared with the cell lines. To identify aptamers with greater B-ALL affinity, the ratio of aptamer to target cells was reduced with subsequent selection rounds to increase competition among the aptamers for any B-ALL epitopes. To enrich for aptamers capable of entering B-ALL cells, the combination of a high-salt (0.5 M NaCl) wash with trypsin was used to cleave and disrupt surface-bound aptamer-protein interactions. Nine selection rounds, summarized in Table 1, were performed to enrich for RNA aptamers that selectively internalized into the B-ALL cell lines.

Changes in aptamer library complexity during B-ALL cell internalization SELEX was monitored using a modified diversity standard of random oligonucleotides (DiStRO) double-stranded DNA (dsDNA) reverse melt curve assay (Figure 2A).[49] During the SELEX process, aptamer libraries become less complex as aptamers within the library shift toward those specific for the target of interest. Assessing this shift in aptamer library complexity helps determine whether the selection pressure applied to the aptamer library is effective and when enough selection rounds have been conducted. To determine relative aptamer library complexity, the dsDNA from each selection round is melted, and the re-annealing efficiency with decreasing temperature is assessed using a dsDNA fluorescent dye. More complex aptamer libraries (e.g., the starting aptamer library) will re-anneal at lower temperatures, whereas less complex aptamer libraries (e.g., selection rounds) will re-anneal at higher temperatures. A significant drop in aptamer library complexity was observed for B-ALL cell internalization SELEX between rounds 3 and 6 and then again between rounds 7 and 8, represented by a shift in the reverse melt curves toward higher temperatures (Figure 2A). No further changes in library complexity were observed between the eighth and ninth selection rounds. These data suggest that the aptamer library was fully converged by round 8, and no additional selection rounds would be potentially beneficial.

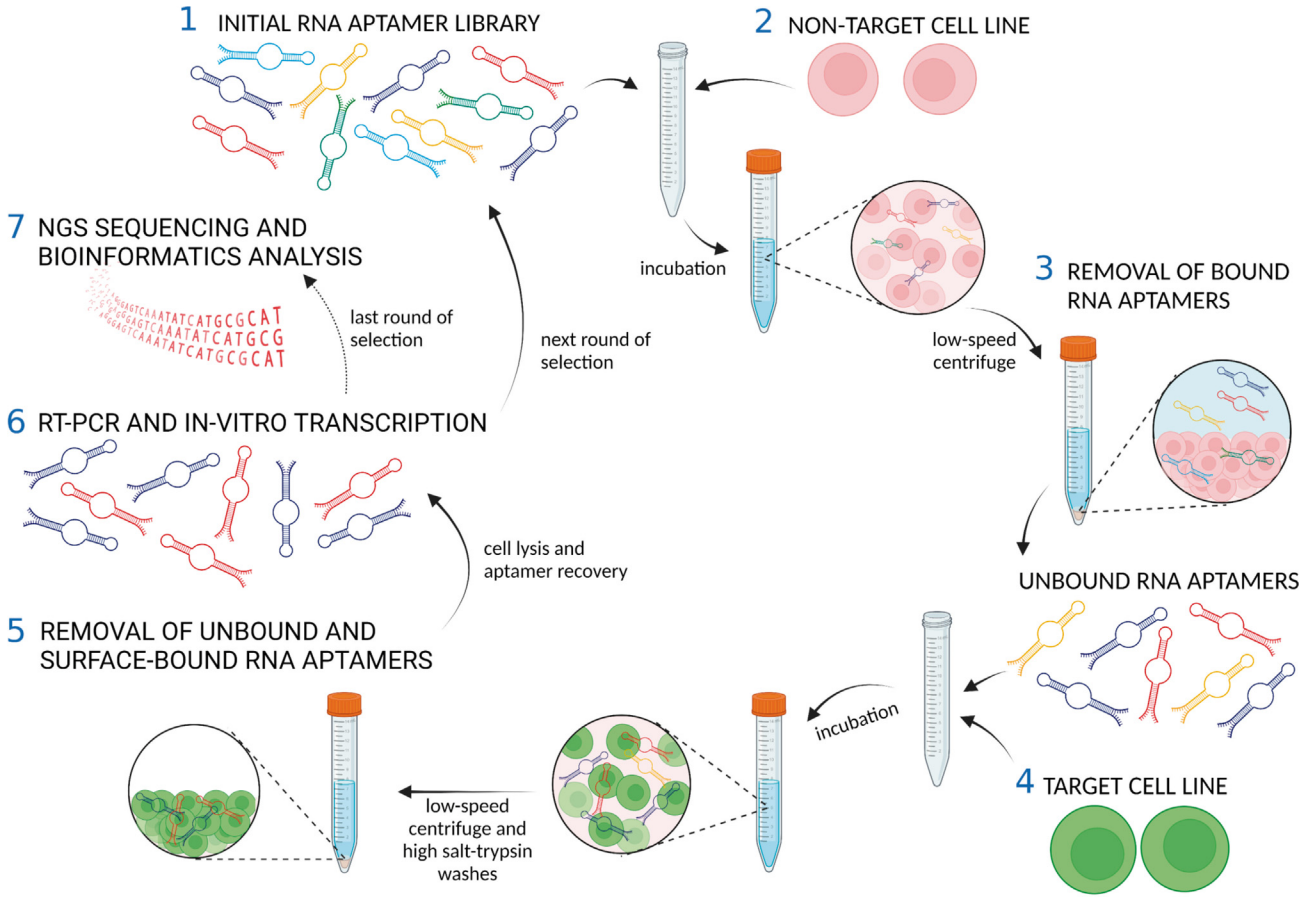

Figure 1. B-ALL cell internalization SELEX for RNA aptamer selection

Cell internalization SELEX was modified for non-adherent cells by utilizing low-speed centrifugation to pellet cells and change solutions. Selection pressure to identify internalizing aptamers was applied using a high-salt (0.5 M NaCl) wash with trypsin. The recovered RNA aptamers were amplified using RT-PCR and *in vitro* transcribed to become the aptamer library for the subsequent round of selection.

Next, the specificity of the B-ALL cell internalization SELEX selection rounds for the B-ALL cell lines was assessed using a quantitative reverse-transcriptase PCR (qRT-PCR) aptamer internalization assay (Figure 2B). The starting RNA aptamer library (round 0) and B-ALL cell internalization SELEX aptamer libraries from selection rounds (2, 4, 6, 7, 8, and 9) were incubated with either the B-ALL KOPN-8 cell line or a non-target cell line (Jurkat or Ea.Hy926), and the internalized aptamer RNA was quantified by qRT-PCR. The qRT-PCR data suggest that significant B-ALL cell aptamer specificity was achieved between the fourth and sixth selection rounds with introduction of the Jurkat cell line as a negative selection pressure (Table 1; Figure 2B). Aptamer specificity for the B-ALL cell lines appears to increase through round 6 with introduction of the Ea.Hy926 cells as a second negative selection pressure (Table 1; Figure 2B). The greatest aptamer specificity for the B-ALL cell lines was observed by the seventh selection round, with no significant increase in selection rounds 8 and 9 (Figure 2B). These data support the aptamer library complexity data (Figure 2A) showing that the aptamer library had converged by round 7 and that no additional selection rounds were necessary.

Next-generation sequencing of B-ALL cell internalization SELEX selection rounds

The B-ALL cell internalization SELEX selection rounds and the starting aptamer library were sequenced by next-generation sequencing (NGS). A total of 7,888,283 raw reads were obtained with an average of 717,116 reads per selection round (Table S1). Using a Galaxy workflow, raw reads were processed and compiled into a non-redundant database consisting of 4,216,070 unique aptamer sequences observed across all selection rounds and the starting aptamer library (round 0).[50] From these data, the overall sequence enrichment (Figure 2C) of each selection round was calculated: sequence enrichment = 100 × (1 − [number of unique sequences / number of total sequences]). A significant increase in sequence enrichment was observed from the second through the fifth selection rounds, with a plateau in sequence enrichment following the sixth selection round. These findings with the NGS data confirm the DiStRO dsDNA reverse melt curve and qRT-PCR results in Figures 2A and 2B showing that the aptamer library converged by the seventh selection round during B-ALL cell internalization SELEX.

Aptamers enriched during the SELEX process will exhibit an increase in persistence (defined as continued or prolonged existence of aptamers across multiple selection rounds) and abundance (defined as unique aptamer duplicate reads within selection rounds). Two Galaxy workflows (abundance non-redundant database [NrD] analysis workflow and persistence NrD analysis workflow) were used to analyze the persistence and abundance of unique aptamer sequences compiled in the B-ALL cell internalization SELEX non-redundant database.[50] The persistence analysis determines the round representation as the number of selection rounds in which each unique aptamer sequence is observed (Figure S1A), and the abundance analysis determines the distribution of aptamer read counts within each selection round (Figure S1B). Round representation and aptamer abundance from round 1 through round 4 increased significantly compared with round 0. To identify B-ALL cell internalization SELEX-selected aptamers, we filtered potentially selected aptamers from non-selected aptamers as those exhibiting significantly greater round representation and abundance compared with round 0. An aptamer round representation of 3 and an aptamer abundance read count of at least 6 were used. In the B-ALL cell internalization SELEX selection rounds, 1,208 unique aptamer sequences were observed in 3 or more selection rounds and had a read count of at least 6, whereas only 15 unique aptamer sequences in round 0 met the same criteria (Figures S1A and S1B).

Table 1. B-ALL cell internalization SELEX conditions

Round	Non-target cell line	Time	Target cell line	Cell number	Time
1	no cells	15 min	KOPN-8	15×10^6	30 min
2	no cells	15 min	NALM-16	15×10^6	30 min
3	Jurkat	15 min	KOPN-8	15×10^6	30 min
4	Jurkat	15 min	NALM-16	15×10^6	30 min
5	Jurkat + Ea.Hy926	15 min	KOPN-8	15×10^6	30 min
6	Jurkat + Ea.Hy926	15 min	NALM-16	15×10^6	30 min
7	Jurkat + Ea.Hy926	15 min	KOPN-8	5×10^6	30 min
8	Jurkat + Ea.Hy926	15 min	NALM-16	5×10^6	30 min
9	Jurkat + Ea.Hy926 + WBCs from healthy donor	15 min	KOPN-8	5×10^6	30 min

The RNA aptamer library was incubated only with B-ALL cells (target cell lines) in the first two rounds. The cell internalization SELEX process starts with incubation of the RNA aptamer library with the non-target cell line (from round 3) for 15 min with each cell line. To recover unbound aptamers, cells were pelleted using low-speed centrifugation, and the supernatant was recovered. Then, the recovered RNA library was incubated with the target cell line for 30 min. B-ALL cells were washed off three times using low-speed centrifugation. Finally, B-ALL cells were lysed, and the internalized aptamers were recovered and amplified by RT-PCR for subsequent rounds of selection.

Identification of candidate aptamers from B-ALL cell internalization SELEX

Several aptamer research groups have reported that aptamers with the highest read numbers were not necessarily the highest-affinity aptamers.[22,31,51,52] Rather, observations suggests that the higher-affinity aptamers exhibited the greatest fold enrichment during SELEX or with changes in selection pressure during SELEX. Changes in enrichment were determined for each of the 1,208 unique aptamers; specifically, after addition of negative selection pressure (Table 1) using Jurkat cells (after round 3) and Ea.Hy926 cells (after round 5), with the greatest decrease in aptamer library complexity (Figure 2A, rounds 3–6), with the greatest increase in aptamer library specificity (Figure 2B, rounds 4–6), and with the greatest increase in aptamer library enrichment (Figure 2C, rounds 2–5).

Next, the 1,208 aptamers were analyzed using an unpublished updated version of an aptamer clustering algorithm that examines sequence (Figure S2) and structural (Figure S3) relatedness with the premise that related aptamers will bind the same epitope.[38] The sequence enrichment data were then mapped onto the clustering results to determine which groups of related aptamers exhibited an increase in enrichment. From each cluster of related aptamers, representative candidate aptamers were identified. Larger clusters of aptamers were examined more closely for groups of aptamers within the cluster that had the same predicted structure (Figures S2B, S3B, and S3C). From the sequence and structure analysis and aptamer enrichment analysis, we identified 38 B-ALL candidate aptamers (Table S2).

In addition to B cell selectivity, we were interested in identifying aptamers specific for CD22 because it plays a critical role in B-ALL therapeutics because of its restricted expression on B cells and internalizing properties.[8,53,54] Furthermore, the positive selection cell lines (NALM-16 and KOPN-8) used during the B-ALL cell internalization SELEX, but not the negative cell lines (JURKAT and Ea.Hy926), express CD22.[55] Therefore, we hypothesized that a screening strategy using molecular docking and molecular dynamics could be useful to identify a subset of the 38 candidates that is enriched for those that might bind CD22.

Molecular docking and molecular dynamics studies of B-ALL cell internalization SELEX candidate aptamers

CD22 is a transmembrane glycoprotein with seven immunoglobulin (Ig)-like domains (d1–d7).[56–59] Ereño-Orbea et al.[9] solved the full-length extracellular domain structure of CD22 (d2–d3 region). To determine whether one or more of our 38 B-cell aptamer candidates are predicted to target the d2–d3 region of CD22, a docking study followed by atomistic molecular dynamics was conducted to predict the number of hydrogen bonds (H-bonds) between each aptamer candidate and the CD22 d2–d3 region. The H-bond analysis has been applied to describe the strength of protein-ligand[60] and protein-protein[61] interactions and can be used to predict the strength of potential aptamer-protein interactions. Docking was conducted with PatchDock,[62] and systems were prepared for molecular dynamics using the Solution Builder from the CHARMM-GUI[63–65] web server. All structures were inspected using Visual Molecular Dynamics (VMD).[66] Unbiased molecular dynamics simulations were run for all structures, and H-bonds were analyzed with GROMACS[67] (gmx_hbond function). The 38 candidate aptamers were ranked (B-ALL aptamers 1–38) according to the predicted H-bond number (Figure 3A), and the top five were identified for further study (B-ALL aptamers 1–5).

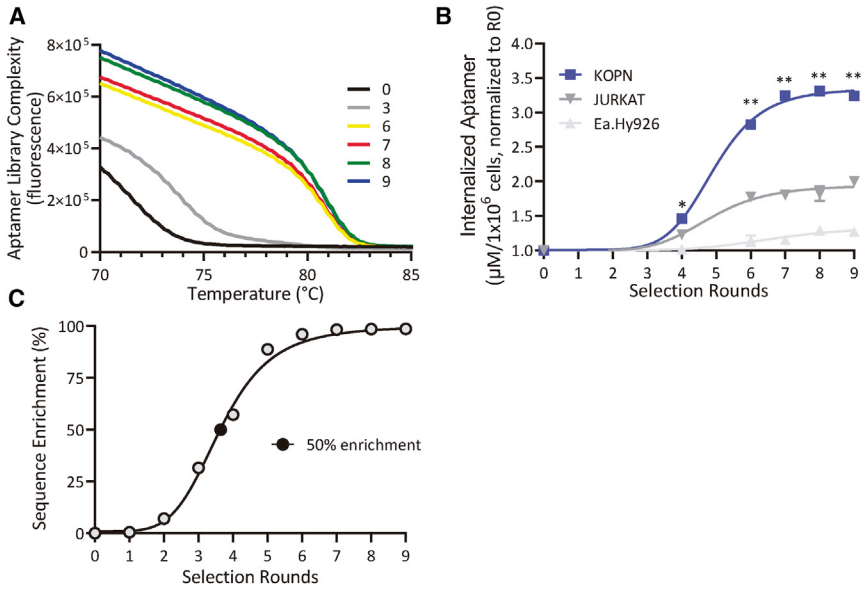

Figure 2. Analysis of B-ALL cell internalization SELEX selection rounds

(A) A DiStRO DNA reverse melt curve assay for aptamer library complexity was used to monitor progression of the B-ALL cell internalization SELEX process. (B) A qRT-PCR aptamer internalization assay was used to determine the cell specificity of the B-ALL cell internalization selection rounds. Aptamer RNA selection rounds 0, 2, 4, and 6–9 were tested for cell-specific internalization into the KOPN-8, Jurkat, and Ea.Hy926 cell lines. Data are plotted with mean ± SEM; n = 3 biological replicates; 2-way ANOVA, $p < 0.001$ with Tukey's multiple-comparisons post hoc test, KOPN versus Jurkat or Ea.Hy926, *$p < 0.05$, **$p < 0.0001$. (C) The sequence enrichment from NGS data attained from the B-ALL cell internalization SELEX selection rounds was calculated as the complement of the percentage of unique reads relative to the total reads: sequence enrichment = 100 × (1 −[number of unique sequences / number of total sequences]).

Specificity of the B-ALL aptamers for B-ALL cell lines NALM-16 and KOPN-8

The cell specificities of the candidate B-ALL aptamers (aptamers B-ALL1–B-ALL5) were evaluated using the same qRT-PCR internalization assay used to examine the B-ALL cell internalization SELEX selection rounds (Figure 2B). In addition to the B-ALL aptamers predicted to target CD22, one B-ALL aptamer (aptamer B-ALL31) that was not predicted to bind the CD22 d2–d3 region but exhibited significant enrichment throughout B-ALL cell internalization SELEX was also evaluated (Figure 3A; Table 2). To serve as a negative control, we identified one aptamer that was only observed in round 0 but not in any of the selection rounds and did not have any sequence/structure similarity to any of the candidate aptamers (aptamer control) (Table 2).

The B-ALL cell lines NALM-16 and KOPN-8 and negative cell lines Jurkat and Ea.Hy926 were treated with each aptamer (50 nM), and aptamer internalization was evaluated by qRT-PCR. Aptamers B-ALL1, B-ALL2, B-ALL3, B-ALL4, and B-ALL31 showed significant specificity for NALM-16 cells over both negative cell lines (Figure 4A). Aptamer B-ALL5 trended toward specificity for NALM-16 cells over the negative cell lines, but this difference was not found to be significant ($p = 0.0582$ versus Jurkat, $p = 0.0645$ versus Ea.Hy926). The control aptamer exhibited no specificity for NALM-16 cells or either negative cell line ($p > 0.5$). However, only two of the candidate aptamers, B-ALL1 and B-ALL2, showed specificity for KOPN-8 cells compared with either negative cell line (Figure 4A). To corroborate these results, the dose dependence of aptamers B-ALL1 and B-ALL2 for the B-ALL cell lines against the negative cell lines was evaluated. We observed significantly greater dose-dependent internalization of aptamers B-ALL1 and B-ALL2 for the NALM-16 and KOPN-8 cell lines compared with either negative cell line (Figure 4B; Tables S3 and S4).

B-cell aptamer interaction with CD22 protein

To test the interaction of the B-ALL aptamers with CD22, we attempted to silence CD22 expression of the NALM-16 and KOPN-8 cell lines; however, we and others have observed that these B-cell lines are difficult to transfect by most methods (Figure S4).[68–70] As an alternative, we treated Chinese hamster ovary (CHO) cells either expressing human CD22 (CHO 22+) or wild-type CHO cells (CHO WT)[71–74] that do not express CD22 (Figure S5) with each candidate aptamer and determined by qRT-PCR the amount of internalized aptamer. Aptamer B-ALL1 exhibited significantly greater binding for CHO cells expressing CD22 than for CHO WT cells (Figure 5A). No significant difference was observed between CHO WT and CHO 22+ cells with any of the other aptamers tested. To verify the interaction between aptamer B-ALL1 and CD22, the dose dependence of aptamer B-ALL1 was assessed for the CHO 22+ cells and CHO WT cells. Aptamer B-ALL1 dose dependence was found to be significantly greater for the CHO 22+ cells than CHO WT cells (Figure 5B). To further support that aptamer B-ALL1 could target CD22, this aptamer was tested against CHO CD22+ cells treated with siRNAs that silence CD22 gene expression (Figure 5C). Significantly reduced aptamer B-ALL1 internalization was observed with CHO CD22+ cells treated with CD22 siRNAs compared with aptamer B-ALL2 and the control aptamer (Figures 5C and 5D). Finally, to investigate the selectivity of our candidates, we performed a CD22 binding assay experiment, measuring the amount of recovered aptamer incubated with CD22 protein and equimolar concentrations of control human IgG1 or epratuzumab IgG1, which also binds in the d2–d3 region of CD22.[9] Our results revealed specific binding of the B-ALL1 aptamer for histidine-tagged CD22 compared with the control aptamer and the control histidine-tagged protein (Figure 5E). The B-ALL1 aptamer displayed no significant competition with epratuzumab for CD22, although a possible trend was observed (Figure 5E). Together, these data support our theory that aptamer B-ALL1 interacts with human CD22 expressed by B-ALL cells.

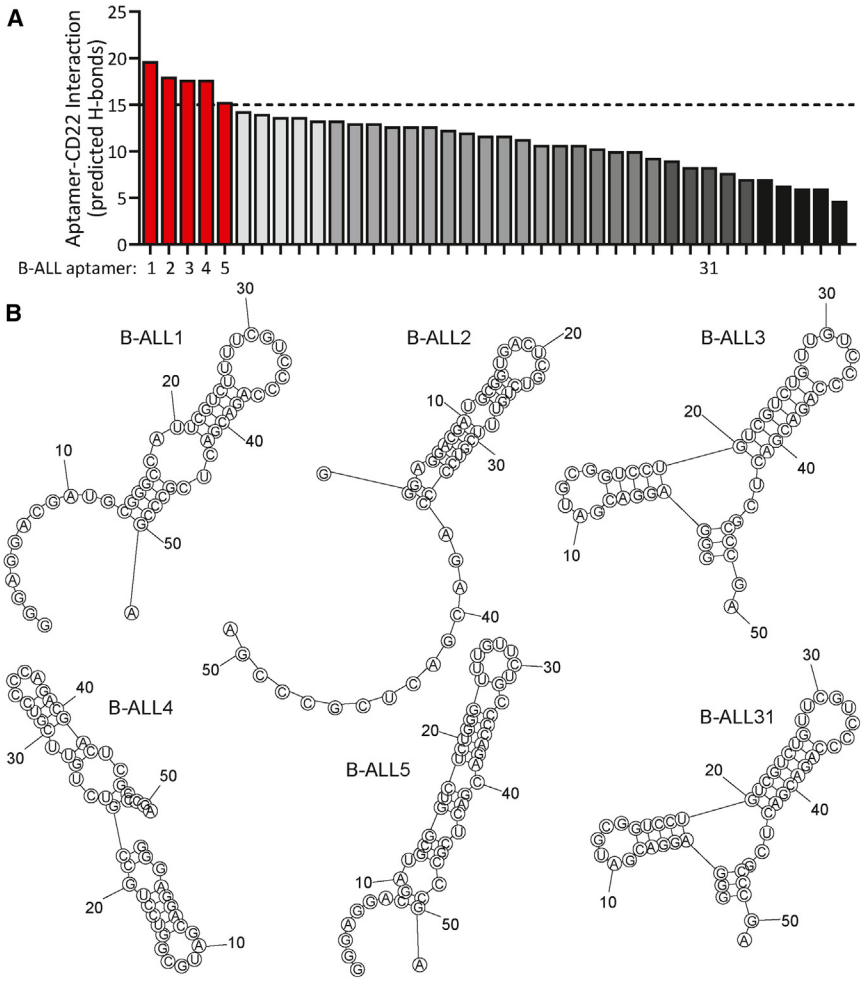

Figure 3. *In silico* docking between CD22 and candidate aptamers

(A) The number of H-bonds after 30 ns of molecular dynamics simulation between candidate B cell aptamers and the epratuzumab region of the CD22 protein. The top five selected candidates (aptamers B-ALL1–B-ALL5), and the most abundant aptamer observed during B-ALL cell internalization SELEX (aptamer B-ALL31) were identified (red) for experimental validation. (B) Predicted secondary structure of aptamers B-ALL1–B-ALL5 and B-ALL31 using the RNA structure.[109]

DISCUSSION

B-ALL cell internalization SELEX identified two RNA aptamers, aptamers B-ALL1 and B-ALL2, that selectively internalize into B-ALL cells. Of these two B-cell-specific aptamers, the B-ALL1 aptamer was found to interact with the CD22 receptor. Aptamer B-ALL1 was observed to target CD22-expressing CHO cells in a dose-dependent manner, which could be prevented by siRNA-mediated silencing of CD22 expression. The interaction of B-ALL1 and CD22 was confirmed in a binding assay with recombinant CD22. Together, these data suggest that the B cell aptamer B-ALL1 targets CD22 and internalizes into B cells. Aptamers have been developed against CD19[75,76] and CD20,[77] but B-ALL1 is the first documented aptamer that targets CD22. CD22 is present in nearly 90% of patients with B-ALL and is involved in B cell receptor (BCR) activation and regulation.[8,78–80] Therefore, identification of aptamer B-ALL1 represents a significant advancement in aptamers capable of targeting B-ALL. Future studies with these B cell-specific aptamers could potentially yield safer and more efficacious treatments for B-ALL.[81,82]

To isolate the B cell-specific aptamers, we applied cell internalization SELEX modified for suspension cells coupled with NGS and a novel bioinformatic strategy to identify aptamers specific for CD22. Our SELEX strategy was based on previous methods that alternate between human and porcine thrombin during selection rounds to produce thrombin-specific aptamers that bound both species with high affinity.[83] Thus, we "toggled" different B-ALL cell subtypes to ensure that the selected aptamers would target proteins conserved between the different B-ALL cells. A DNA melt assay and cell internalization assay indicated that the B cell cell internalization SELEX plateaued by round 6 and was completed by round 9. NGS aptamer sequence enrichment data confirmed these results. However, although the sequence enrichment data suggested no changes following round 6, we did observe a decrease in B-ALL1 aptamer read counts in the last round of selection. We believe this is possibly due to the hWBC preparations containing B cells with high levels of CD22 expression. The aptamer persistence and abundance analysis identified 1,208 unique "true-selected" aptamer sequences from the 4,216,070 unique aptamer sequences found by NGS. These 1,208 unique aptamer sequences were clustered by sequence and structure similarity, from which 38 candidates were identified that exhibited positive enrichment during B-ALL cell internalization SELEX.

We employed a molecular docking and molecular dynamics strategy to rank the pool of 38 aptamer candidates for any that might target CD22. Previous molecular docking and molecular dynamics research has focused on understanding aptamer-protein binding after aptamer selection and characterization.[85,86] Generally, these techniques have been used for optimizing aptamer stability and specificity for its target protein.[87,88] Drawing on strategies that have been applied successfully for other protein-ligand interactions,[60,61,84] we ranked our aptamer candidates based on the number of predicted H-bonds with the d2–d3 ectodomains of the CD22 protein that includes the epratuzumab epitope.[9] The highest-ranked aptamer, B-ALL1, was specific for CD22 based on cell internalization and *in vitro* binding assays. These results demonstrate the potential of applying molecular docking and molecular dynamics to narrow down aptamer candidates from NGS

Table 2. CD22-specific candidate aptamers

Aptamer	RNA aptamer sequence (5′-3′)	Minimum free energy (MFE)	Ensemble probability[a]	Ensemble diversity[b]
B-ALL 1	GGG AGG ACG AUG CGG GCC AUU CGU CUU UUC GUC CCC AGA CGA CUC GCC CGA	18.03	0.51	5.99
B-ALL2	GGG AGG ACG AUG CGG UGA CUC GUC UGU UUC GUC CCC AGA CGA CUC GCC CGA	15.59	0.18	15
B-ALL 3	GGG AGG ACG AUG CGG UCC UGU CGU CUG UUG UCC CCA GAC GAC UCG CCC GA	25.87	0.75	0.18
B-ALL 4	GGG AGG ACG AUG CGG UCC UGC CGU CUG UUC GUC CCC AGA CGA CUC GCC CGA	22.04	0.37	6.76
B-ALL 5	GGG AGG ACG AUG CGG UCU CUG GGU UUG UUC UGC CCC AGA CGA CUC GCC CGA	19.34	0.27	4.64
B-ALL31	GGG AGG ACG AUG CGG UCC UGU CGU CUG UUC GUC CCC AGA CGA CUC GCC CGA	26.45	0.75	0.17
Control	GGG AGG ACG AUG CGG UCC CAC GAG UGG UUU UCG UAC AGA CGA CUC GCC CGA	19.3	0.65	0.89

[a]Ensemble probability as calculated by RNAfold[101] refers to the probability of a sequence to be represented by a single structure in the Boltzmann weighted ensemble set of all possible structures.

[b]"Ensemble diversity" as calculated by RNAfold[101] is the average base-pair distance between all structures in the thermodynamic ensemble and estimates the complexity of the structural ensemble. Low ensemble diversity indicates fewer possible structures, while higher ensemble diversity suggests a greater number of possible structures.

data for experimental evaluation. However, one important consideration is that any molecular docking study will be limited by the available crystal structure. For example, the CD22 extracellular domain is comprised of seven Ig ectodomains (d1–d7).[9] Therefore, any aptamers that interact with CD22 outside of the d2–d3 region would have been missed by our docking study. Despite this limitation, we envision that molecular docking can streamline traditional screening that may be useful in research settings that are limited to screening a small number of candidates.

The *in vitro* binding assay indicates that the B-ALL1 aptamer interacts with the histidine-tagged CD22; however, only a non-significant trend toward competition between the B-ALL1 aptamer and epratuzumab IgG1 for CD22 was observed. These binding data and the results from the docking study suggest that the B-ALL1 aptamer binds CD22 within the d2–d3 ectodomains and that the B-ALL1 aptamer targets an epitope separate from epratuzumab. Interestingly, the observed trend of reduced B-ALL1 aptamer binding in the presence of epratuzumab suggests a possible indirect interference between them. Epratuzumab binding could alter the confirmation of CD22 in a manner that changes the interaction of the B-ALL1 aptamer with CD22. Additional experiments will be necessary to test these possibilities and to determine the precise binding site of the B-ALL1 aptamer in the CD22 protein.

Interestingly, aptamer B-ALL1 was the 573rd-ranked aptamer in the NGS non-redundant database. Our results with the B-ALL1 aptamer support the theory that less abundant aptamers in an aptamer NGS dataset can be of significant interest.[38,50] Without a more in-depth bioinformatics analysis that included clustering for groups of aptamers related by sequence and/or structure and the CD22 docking study, aptamer B-ALL1 would have been overlooked if we had only selected the top five aptamers with the highest read counts for further characterization. Based on these results, a more in-depth bioinformatics analysis, such as molecular docking, should be considered when identifying ideal aptamer candidates for further *in vitro* studies.

We observed that aptamers B-ALL1 and B-ALL2 exhibited specificity for the NALM-16 pre-B ALL cell line and the KOPN-8 common B-ALL cell line. These results imply that pre-B-ALL and common B-ALL share common membrane proteins, like CD22, that are not expressed by either negative cell line. However, several of the B cell aptamers (aptamers B-ALL31, B-ALL3, B-ALL4, and B-ALL5) that were anticipated to be specific across both B cell lines showed only specificity for the NALM-16 pre B-ALL cell line but not the KOPN-8 common B cell line. One plausible explanation for this discrepancy of aptamer specificity between the two B cell lines is that the membrane proteins associated with ALL may vary in number and composition across tumor subtypes for hematological malignancies. Because of the lack of information about the cellular uptake mechanism of aptamers,[89,90] we also cannot exclude the possibility that changes in the processing and endosomal escape mechanisms may present additional confounding variables. The rate of access to the cytosol for internalizing aptamers mainly depends on the rate of receptor recycling and endosomal escape efficiency, which may be different for distinct B-ALL subtypes. While we believe these limitations have not impacted the primary outcome of this study, these results suggest the critical importance of accurate ALL subtype characterization with ALL-targeted therapeutics and imply that each B-ALL subtype may be best targeted separately. Specific tumor subtype targeting has already proven to be useful for breast cancer aptamer development, with aptamers generated against triple-negative breast cancer cells,[31] HER2-positive breast cancer cells,[91] and estrogen-progesterone-glucocorticoid-positive breast cancer cells.[92] Future efforts regarding ALL aptamer development include use of specific ALL subtypes when designing the SELEX strategy.

Finally, although aptamers B-ALL1 and B-ALL2 were specific across both B cell lines, our results demonstrated that only aptamer B-ALL1 significantly improved binding toward CD22 protein. This implies that aptamer B-ALL2 may be binding to another cell-surface receptor in B-ALL cells. While these studies focused on the initial *in vitro* proof

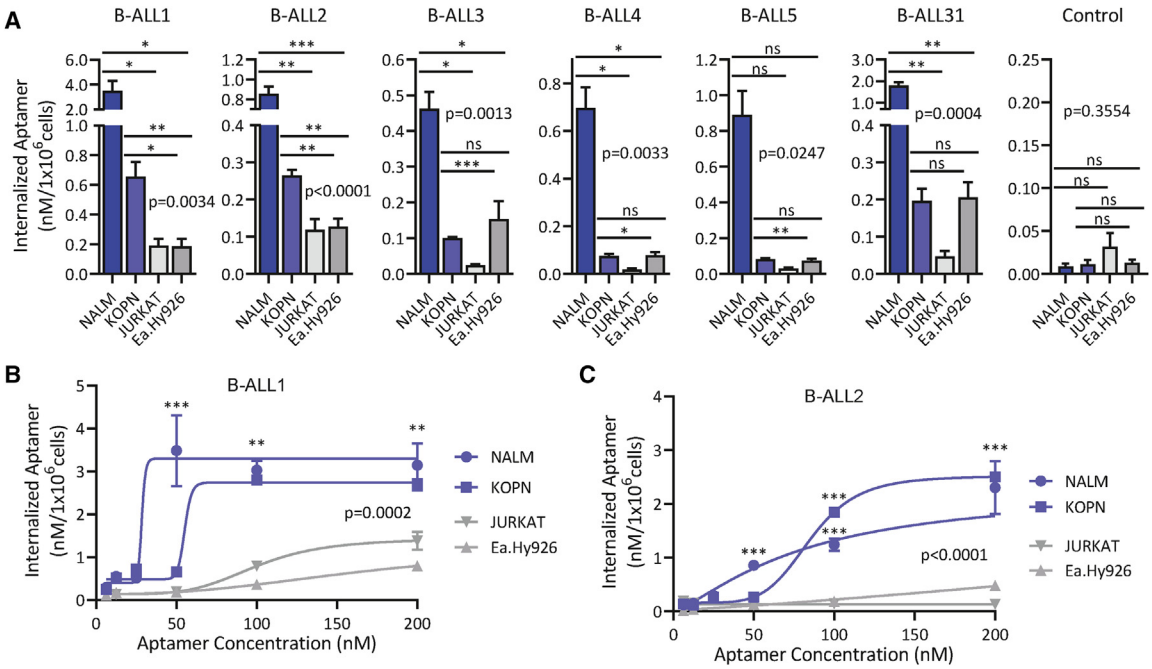

Figure 4. Specificity of the B cell aptamers for the B-ALL NALM-16 and KOPN-8 cell lines

(A) Aptamer qRT-PCR internalization assay of the B-ALL aptamers and a negative control aptamer. B-ALL cell lines NALM-16 (NALM) and KOPN-8 (KOPN) and negative cells lines (Jurkat and Ea.Hy926) were treated with 50 nM of each aptamer. Data are plotted with mean ± SEM; n = 4–8 biological replicates; Brown-Forsythe and Welch ANOVA with Dunnett's T3 multiple-comparisons post-hoc test for NALM or KOPN versus JURKAT or Ea.Hy926. The p values are displayed on the graph. *p < 0.05, **p < 0.01, ***p < 0.001; ns, not significant. Shown is the dose-dependent qRT-PCR internalization assay of aptamers (B) B-ALL1 and (C) B-ALL2. Data are plotted as mean ± SEM; n = 4–8 biological replicates; 2-way ANOVA with Tukey's multiple-comparisons post hoc test for NALM or KOPN versus Jurkat or Ea.Hy926. The p values are displayed on the graph. **p < 0.001, ***p < 0.0001.

of concept, studies that evaluate the *in vivo* target specificity of the B-ALL1 aptamer are warranted. Also, further research should be undertaken to investigate the real power of molecular docking and molecular dynamics as a screening strategy for aptamers. In summary, we combined cell internalization SELEX with advanced computational tools to enable rapid identification of RNA aptamers specific for B-ALL, including one aptamer that specifically targets CD22.

MATERIALS AND METHODS

Cell culture

The Jurkat (ATCC, TIB-152), KOPN-8 (Deutsche Sammlung von Mikroorganismen und Zellkulturen [DSMZ], ACC 552), and NALM-16 (DSMZ, ACC 680) cell lines were kindly provided by Dr. Miles A. Pufall and Dr. Carlos Chan from the University of Iowa (Iowa City, IA, USA). Jurkat, KOPN-8, and NALM-16 cells were maintained in RPMI-160 medium (Gibco, 11875119) supplemented with 10% fetal bovine serum (FBS) (Atlanta Biologicals, S11550). Ea.Hy926 cells (ATCC, CRL-2922) were cultured in Dulbecco's modified Eagle's medium (DMEM; Gibco, 11965092) supplemented with 10% FBS. CHO WT and CHO 22+ cells were generously provided by Dr. James C. Paulson (The Scripps Research Institute (La Jolla, CA, USA). CHO WT and CHO 22+ cells were prepared as described previously.[71,72] CHO WT and CHO 22+ cells were maintained in DMEM/F12 (Gibco, 11320033) supplemented with 10% FBS and DMEM/F12 supplemented with 10% FBS and 500 μg/mL Hygromycin-B (Roche, 10843555001), respectively. Cell lines were incubated at 37°C under 5% CO_2 with medium changes every 2–3 days until confluent. Non-adherent cells were trypsinized using trypsin EDTA (0.25%; Gibco, 25200072). Cell lines were screened for mycoplasma contamination[93] and used within eight passages.

Isolation of WBCs

After informed consent, blood (12 mL) was obtained from two healthy donors without any exclusion criteria. Blood was diluted 1:2 with PBS and layered over with 15 mL of Cytiva Ficoll-Paque PLUS (Thermo Fisher Scientific, 11778538). WBCs were collected according to the Ficoll-Paque manufacturer's instructions. Cells were resuspended in RPMI-1640 medium and used within 2 h after extraction.

Cell internalization SELEX

The initial (round 0) aptamer library was attained as a Sel2N20 template oligo (5′-TCGGGCGAGTCGTCTG-N20-CCGCATCGTCCTCCC-3′) (Integrated DNA Technologies, Coralville, IA, USA). The template oligo was extended after annealing with the Sel2-5′ primer (5′- TAATAC GACTCACTATAGGGAGGACGATGCGG-3′). The extended dsDNA was *in vitro* transcribed using Y639F mutant T7 RNA polymerase using 2′-fluoro-modified pyrimidines (TriLink Biotechnologies, 2′-fluoro-2′-deoxycytidine triphosphate (dCTP), N-1008; 2′-fluoro-2′-deoxyuridine

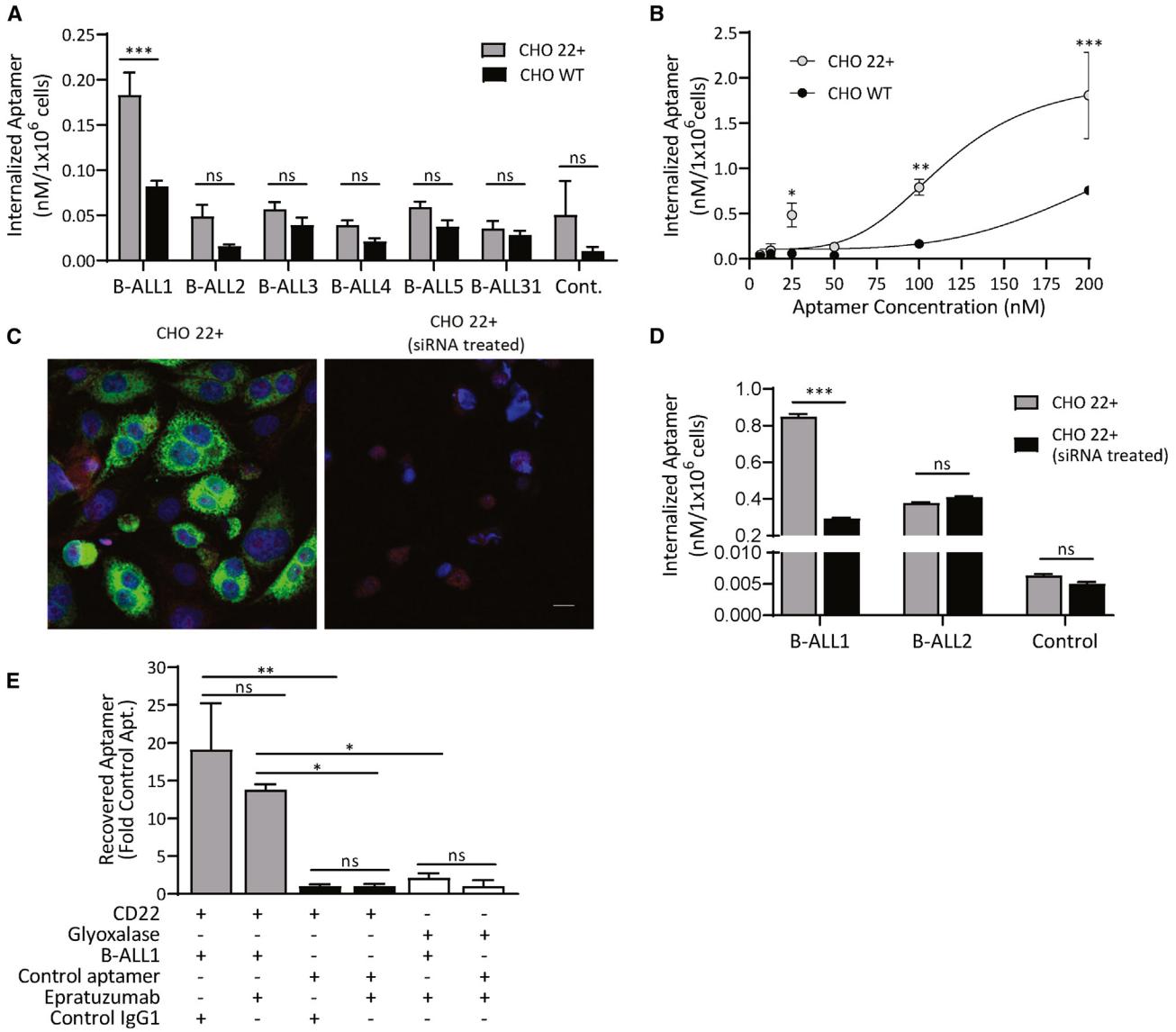

Figure 5. B cell aptamer interaction with CD22 protein

(A) B-ALL aptamer (B-ALL1–B-ALL5 and B-ALL31) and control aptamer (Cont.) specificity for CD22 was evaluated using an aptamer qRT-PCR internalization assay with CHO cells expressing CD22 (CHO 22+) and wild-type CHO cells not expressing CD22 (CHO WT). Data are plotted as mean ± SEM; n = 3 biological replicates; mixed effect analysis $p > 0.005$ with post hoc Bonferroni's multiple-comparisons test; ***$p < 0.0001$. (B) Dose dependence of B cell aptamer B-ALL1 and Cont. aptamer for CD22. Data are plotted as mean ± SEM; n = 3 biological replicates; 2-way ANOVA, $p < 0.0001$ with Sidak's multiple-comparisons post hoc test; *$p < 0.05$, **$p < 0.001$, ***$p < 0.0001$. (C) Knockdown of CD22 expression by treatment with anti-CD22 siRNAs. CD22 was detected by anti-human CD22 (green), the cytoplasm was stained with AF568-phalloidin (red), and the nucleus was visualized by TOPRO-3 (blue). Scale bar, 20 μm. (D) qRT-PCR aptamer internalization assay of aptamers B-ALL1, B-ALL2, and Cont. aptamer with CHO 22+ cells and CHO 22+ (siRNA-treated) cells. Data are plotted as mean ± SEM; n = 3 biological replicates; 2-way ANOVA, $p < 0.0001$ with Bonferroni's multiple-comparisons post hoc test; ***$p < 0.0001$. (E) B-ALL1 aptamer and Cont. aptamer specificity for recombinant histidine-tagged CD22 or control histidine-tagged protein (glyoxalase) in the presence of epratuzumab or a control IgG1 (bevacizumab). Data are plotted as mean ± SEM; n = 4 biological replicates; one-way ANOVA with multiple-comparisons post hoc test; **$p < 0.001$, *$p < 0.05$.

triphosphate (dUTP), N-1010) and unmodified purines as described previously.[22,38,39] The cell internalization SELEX process was modified from a previously reported protocol[22] for suspension cell lines. Aptamer RNA was folded at 1 μM in 1× binding buffer (BB) at 95°C for 7 min, 65°C for 15 min, and 37°C for 30 min (1× BB, 20 mM HEPES [pH 7.4] [Sigma-Aldrich, H3537], 0.15 M NaCl [Sigma-Aldrich, S9888], and 2 mM $CaCl_2$ [Sigma-Aldrich, 21115]). Folded aptamer RNA was diluted to 400 nM in RPMI-1640 serum-free medium with 100 mg/mL yeast tRNA (Invitrogen, 11508736). For the first two rounds, the aptamer RNA library was incubated only with a B-ALL cell line (positive selection step) based on

a predetermined time for maximizing RNA internalization into these cells (Figure S6). From rounds 3–9, the aptamer RNA library was incubated first with a non-specific cell line (negative selection step), followed by a positive selection step. Exact conditions used for each selection round are summarized in Table 1. Following incubation of the RNA aptamer library, B-ALL cells were washed three times with 5 mL ice-cold high salt-trypsin (0.5 M NaCl DPBS(−/−) - 0.25% trypsin) to remove unbound and surface-bound RNA aptamers. Between washes, cells were pelleted at 500 × *g* for 3 min at 4°C. Internalized sequences were recovered by TRIzol extraction (Invitrogen) as reported previously.[22,44] Recovered aptamer RNA was reverse transcribed using the Sel2-3′ primer (5′- TCGGGCGAGTCGTCTG-3′) with Superscript III and PCR amplified using the Sel2-3′ primer and Sel2-5′ primer with a Taq DNA polymerase (Denville Scientific, C775Y42) as described previously.[22,44]

DiStRO dsDNA reverse melt curve assay

Aptamer library complexity was evaluated as described previously[38,94] using 0.5 mM dsDNA from rounds 0, 3, 6, 7, 8, and 9 in triplicate. Samples were combined with iQ SYBR Green Supermix (Bio-Rad, 1708880) at a 1:1 volume and subjected to a reverse DNA melt curve protocol (95°C–25°C, ramp over 20 min) using a quantitative PCR machine (Applied Biosystems QuantStudio 3 Real-Time PCR). Data were plotted as fluorescence (SYBR Green intensity) against increasing temperature (°C).

Aptamer internalization assay by qRT-PCR

Aptamer specificity (selection rounds and single aptamers) were evaluated using an aptamer internalization assay as reported previously with 3–8 biological replicates for each condition tested.[38,43] Cells were treated with folded aptamer RNA, selection rounds, or single aptamers, for 30 min at 37°C under 5% CO_2. Unbound and cell-surface-bound RNA was removed using three ice-cold, high-salt trypsin washes. Internalized aptamer RNA was recovered by TRIzol extraction. When assessing the selection round aptamer libraries, TRIzol was supplemented with 0.5×10^{-3} pmol/mL of Sel1 aptamer (M 12-23 aptamer)[95] as a reference control. A two-step qRT-PCR procedure[38] was used to quantify the amount of recovered aptamer RNA. For reverse transcription, moloney murine leukemia virus (MMuLV) (New England Biolabs, M0253L) was used in experiments assessing the selection rounds, and Superscript III (Thermo Fisher Scientific, 18080044) was used in experiments assessing single aptamers. qPCR was conducted in triplicate for each sample using either SYBR Green Supermix (Bio-Rad, 1725120) or iQ SYBR Green Supermix (Bio-Rad, 1708880). Data were normalized to the Sel1 reference control when applicable and to cell number (1×10^6).

Illumina NGS sample preparation

Aptamer RNA from each selection round was reverse transcribed using Superscript III (Thermo Fisher Scientific, 18080044) and a modified Sel2 3′ Illumina primer (5′-CAA GCA GAA GAC GGC ATA CGA GGA TTC GGG CGA GTC GTC TG-3′) (Integrated DNA Technologies) as described previously.[22] The cDNA was PCR amplified using barcoded Illumina primers (5′-CCG CAT CGT CCT CCC-BARCODE-AGA TCG GAA GAG CGT CGT GTA GGG AAA GAG TGT AGA TCT CGG TGG TCG CCG TAT CAT T-3′). Amplicons were purified by gel extraction, pooled, quantified by bioanalyzer, and sequenced by NGS on an Illumina HiSeq 4000 genome sequencer at the Iowa Institute of Human Genetics, University of Iowa (Illumina-based NGS). Round 0 was sequenced in duplicate to provide more robust baseline data compared with the B-ALL selection rounds.

Bioinformatics analyses

NGS aptamer reads were processed and analyzed using Galaxy workflows[42,50] to isolate only the aptamer variable region and compile a non-redundant database of unique aptamer sequences identified from all selection rounds. Two additional Galaxy workflows (abundance NrD analysis workflow and persistence NrD analysis workflow) were used to examine aptamer persistence and abundance to permit filtering of the non-redundant database for true selected aptamers. An individual aptamer was considered a true selected sequence when persistence was at least three and abundance was at least six. The resulting 1,208 aptamers were ranked based on the log2 fold enrichment between rounds 2 and 5 (R2:R5), R2:R9, R4:R6, and R6:R9.

The 1,208 aptamers were analyzed by sequence similarity (edit distance 1) and structure similarity (tree distance 3) using an unpublished updated version (see Data and code availability) of an aptamer clustering algorithm.[38,94] Cytoscape (v.3.9.0)[96] was used to visualize groups of related aptamers. Alignments of related aptamers were examined using ClustalX (v.2.0)[97] and LocARNA (online),[98] respectively. The number of modifications (substitution, insertion, or deletion) required for two sequences to become identical is known as the "edit distance", while "tree distance" refers to the relatedness of two structures; the lower the tree distance, the more closely related the structures are.[38,99,100]

The secondary structures of RNA aptamers were optimized using the Vienna RNAfold web server (http://rna.tbi.univie.ac.at/cgi-bin/RNAWebSuite/RNAfold.cgi),[101] while three-dimensional structures were built using RNA composer.[102] RNA aptamers were saved as PDB format for H-bond measures. The human CD22 protein structure was downloaded from the PDB database (PDB: 5VKJ).[9] The PatchDock web server (https://bioinfo3d.cs.tau.ac.il/PatchDock/) was employed for docking studies.[103,104] Docking for the RNA aptamer-protein complex was visualized using VMD v.1.9.3.[66] Molecular dynamics simulations for H-bond evaluation were prepared using the Solution Builder from CHARMM-GUI (http://www.charmm-gui.org).[63–65] The RNA aptamer-CD22 complex was solvated using a rectangular box with a distance of 10 nm between the complex and the edge of the box. The solvated system was neutralized by adding potassium chloride ions in the simulation. The results were downloaded, and simulations for all CD22 and RNA aptamer complexes for H-bond measures were carried out for 30 ns each, using the CHARMM36 force field implemented in GROMACS software v.2020.1.[67]

siRNAs

Accell siRNAs against human CD22 (set of 4) were synthesized by Dharmacon (Horizon Discovery, EQ-019501-00-0002). 5× siRNA

buffer (Horizon Discovery, B-002000-UB-100) combined with sterile RNase-free water was used to prepare 1× siRNA buffer. Lyophilized siRNA was reconstituted to 100 μM siRNA solution in 1× siRNA buffer. According to the manufacturer's experimental conditions, siRNA medium was prepared by adding 1 μM siRNA solution to 1× Accell delivery medium (Horizon Discovery, B-005000-100). Finally, cells were incubated either with siRNA medium or Accell delivery medium alone at 37°C with 5% CO_2 for 96 h.

Confocal microscopy

0.03×10^6 CHO cells were plated in an 8-well chamber and cultured until the cells adhered. Cells were fixed with 4% paraformaldehyde for 10 min at 4°C, followed by phosphate-buffered saline (PBS) washes at room temperature. Cells were stained for CD22 using procedures similar to those described previously.[105,106] Cells were incubated with rabbit anti-CD22 antibody (1:100, Abcam, ab246334) in 10% donkey serum overnight at 25°C. After washing with PBS, microscope slides were incubated with a mixture of Alexa Flour 488-conjugated donkey anti-rabbit antibody (1:200, Jackson ImmunoResearch, 711-545-152), Alexa Fluor 568 phalloidin (cytoskeleton staining, 1:200, Thermo Fisher Scientific, A12380), and TO-PRO-3 (nucleus staining, 1:200, Thermo Fisher Scientific, R37170) overnight at 4°C. Stained sections were coverslipped with Prolong Diamond Anti-fade Reagent (Invitrogen-Molecular Probes, P36965) after the final washes with PBS. Samples were imaged with a Carl Zeiss LSM 710 confocal laser-scanning microscope as described previously.[107,108] Sections were scanned sequentially in different channels to separate labels. Images from different channels were assigned a pseudocolor and then superimposed. Confocal images were obtained and processed with software provided with the Carl Zeiss LSM 710.

CD22 binding assay

The CD22 binding assay was adapted from the LIRECAP (ligand-receptor complex-binding aptamer) assay[94] using histidine tag-binding Dynabeads (Thermo Fisher Scientific, 10103D). 50 nM recombinant histidine-tagged human CD22 (Thermo Fisher Scientific, A42609) or 50 nM histidine-tagged human glyoxalase (R&D Systems, 5094 959-GL-02M) and equal molar control human IgG1 (bevacizumab) or epratuzumab IgG1 (Invitrogen, MA5-41703) were incubated with 100 nM B-ALL1 aptamer or control aptamer. Steady-state binding was achieved in 1× BB with 100 μg/mL yeast tRNA and 100 μg/mL BSA (RPI, A30075) after 30 min of rotation at room temperature. Non-specifically bound aptamer was removed with two 5-min rotating room temperature washes and one quick room temperature wash using 1× BB with 0.05% Tween 20. Bound aptamer RNA was recovered by phenol-chloroform extraction and assessed by qRT-PCR.

Statistical analyses

All experiments were conducted with 3–4 biological replicates except for experiments that assess cell specificity of the candidate B-ALL aptamers (aptamers B-ALL 1–5), which accounts for 4–8 biological replicates. Mean and standard error of the mean (SEM) were calculated using either GraphPad Prism 9 or Microsoft Excel 2016. GraphPad Prism 9 software was used to determine the analysis of variance (-ANOVA) and half maximal effective concentration (EC_{50}) curves. We used the equation in GraphPad Prism for [Agonist] vs. response – Variable slope for the EC_{50} curves. Statistical significance was set at a p value less than 0.05.

DATA AND CODE AVAILABILITY

Source data are provided with this paper. Further data supporting the findings of this study are available from the corresponding author upon reasonable request. The unpublished updated version of the aptamer clustering algorithm is available in the GitHub repository (https://github.com/ui-icts/aptamer).

SUPPLEMENTAL INFORMATION

Supplemental information can be found online at https://doi.org/10.1016/j.omtn.2023.07.028.

ACKNOWLEDGMENTS

We thank Dr. Rui Sousa (University of Texas, San Antonio) for his generous gift of the mutant (Y639F) T7 RNAP as well as Dr. Kristina Thiel for critical comments and scientific editing of the manuscript. We would also like to acknowledge the Iowa City VA Medical Center for use of the confocal microscope. This work was supported by grants from the National Institutes of Health to W.H.T. (R01HL139581) and P.H.G. (R01CA138503). Additional support to P.H.G. was from the Mary Kay Foundation (9033-12 and 001-09) and the Roy J. Carver Charitable Trust (RJCCT 01-224). M.B.M. received grants from Agencia-PICT (2017-1968, Argentina), and SECITI-UCCuyo (2017-0388, Argentina). S.V. was supported by ACS-IRG grant IRG-18-165-43 (American Cancer Society administered by HCCC, University of Iowa). D.R.-C. was supported by the Bunge and Born Fund (Jorge Oster scholarship 2017-2018) and Fulbright-Argentinian Ministry of Education scholarship 2022-2023.

AUTHOR CONTRIBUTIONS

D.R.-C., M.B.M., P.H.G., and W.H.T. designed experiments. D.R.-C. and M.N.B. conducted experiments. L.-H.L. performed confocal microscopy experiments. W.H.T. designed and performed the bioinformatic analyses. A.L.D.B. and D.M. designed and performed the molecular docking and molecular dynamics experiments. D.S. assisted with Y639F mutant T7 RNA polymerase extraction. S.V. and W.H.T. carried out CD22 binding assay experiments. D.R.-C., D.M., and W.H.T. analyzed the data and conducted statistical analyses. M.B.M., P.H.G., and W.H.T. contributed reagents and materials. D.R.-C. and W.H.T. wrote the paper. All authors reviewed the manuscript.

DECLARATION OF INTERESTS

P.H.G. is an employee of Wave Life Sciences.

REFERENCES

1. Siegel, R.L., Miller, K.D., Fuchs, H.E., and Jemal, A. (2021). Cancer Statistics, 2021. Ca - Cancer J. Clin. *71*, 7–33. https://doi.org/10.3322/caac.21654.

2. Terwilliger, T., and Abdul-Hay, M. (2017). Acute lymphoblastic leukemia: a comprehensive review and 2017 update. Blood Cancer J. *7*, e577. https://doi.org/10.1038/bcj.2017.53.

3. Cobaleda, C., Vicente-Dueñas, C., and Sanchez-Garcia, I. (2021). Infectious triggers and novel therapeutic opportunities in childhood B cell leukaemia. Nat. Rev. Immunol. *21*, 570–581. https://doi.org/10.1038/s41577-021-00505-2.

4. Huang, F.L., Liao, E.C., Li, C.L., Yen, C.Y., and Yu, S.J. (2020). Pathogenesis of pediatric B-cell acute lymphoblastic leukemia: Molecular pathways and disease treatments. Oncol. Lett. *20*, 448–454. https://doi.org/10.3892/ol.2020.11583.

5. Dobson, S.M., García-Prat, L., Vanner, R.J., Wintersinger, J., Waanders, E., Gu, Z., McLeod, J., Gan, O.I., Grandal, I., Payne-Turner, D., et al. (2020). Relapse-fated latent diagnosis subclones in acute B lineage leukemia are drug tolerant and possess distinct metabolic programs. Cancer Discov. *10*, 568–587. https://doi.org/10.1158/2159-8290.CD-19-1059.

6. Jasinski, S., De Los Reyes, F.A., Yametti, G.C., Pierro, J., Raetz, E., Carroll, W.L., and Carroll, W.L. (2020). Immunotherapy in Pediatric B-Acute Lymphoblastic Leukemia: Advances and Ongoing Challenges. Paediatr. Drugs *22*, 485–499. https://doi.org/10.1007/s40272-020-00413-3.

7. Brivio, E., Baruchel, A., Beishuizen, A., Bourquin, J.P., Brown, P.A., Cooper, T., Gore, L., Kolb, E.A., Locatelli, F., Maude, S.L., et al. (2022). Targeted inhibitors and antibody immunotherapies: Novel therapies for paediatric leukaemia and lymphoma. Eur. J. Cancer *164*, 1–17. https://doi.org/10.1016/j.ejca.2021.12.029.

8. Lanza, F., Maffini, E., Rondoni, M., Massari, E., Faini, A.C., and Malavasi, F. (2020). CD22 expression in B-cell acute lymphoblastic leukemia: Biological significance and implications for inotuzumab therapy in adults. Cancers *12*, 303. https://doi.org/10.3390/cancers12020303.

9. Ereño-Orbea, J., Sicard, T., Cui, H., Mazhab-Jafari, M.T., Benlekbir, S., Guarné, A., Rubinstein, J.L., and Julien, J.P. (2017). Molecular basis of human CD22 function and therapeutic targeting. Nat. Commun. *8*, 764. https://doi.org/10.1038/s41467-017-00836-6.

10. Shah, N.N., and Sokol, L. (2021). Targeting CD22 for the Treatment of B-Cell Malignancies. ImmunoTargets Ther. *10*, 225–236. https://doi.org/10.2147/itt.s288546.

11. Kantarjian, H.M., Su, Y., Jabbour, E.J., Bhattacharyya, H., Yan, E., Cappelleri, J.C., and Marks, D.I. (2018). Patient-reported outcomes from a phase 3 randomized controlled trial of inotuzumab ozogamicin versus standard therapy for relapsed/refractory acute lymphoblastic leukemia. Cancer *124*, 2151–2160. https://doi.org/10.1002/cncr.31317.

12. Shah, N.N., Bhojwani, D., August, K., Baruchel, A., Bertrand, Y., Boklan, J., Dalla-Pozza, L., Dennis, R., Hijiya, N., Locatelli, F., et al. (2020). Results from an international phase 2 study of the anti-CD22 immunotoxin moxetumomab pasudotox in relapsed or refractory childhood B-lineage acute lymphoblastic leukemia. Pediatr. Blood Cancer *67*, e28112. https://doi.org/10.1002/pbc.28112.

13. Raetz, E.A., Cairo, M.S., Borowitz, M.J., Lu, X., Devidas, M., Reid, J.M., Goldenberg, D.M., Wegener, W.A., Zeng, H., Whitlock, J.A., et al. (2015). Re-induction Chemoimmunotherapy with Epratuzumab in Relapsed Acute Lymphoblastic Leukemia (ALL): Phase II Results from Children's Oncology Group (COG) Study ADVL04P2. Pediatr. Blood Cancer *62*, 1171–1175. https://doi.org/10.1002/pbc.25454.

14. Zanetti, S.R., Velasco-Hernandez, T., Gutierrez-Agüera, F., Díaz, V.M., Romecín, P.A., Roca-Ho, H., Sánchez-Martínez, D., Tirado, N., Baroni, M.L., Petazzi, P., et al. (2022). A novel and efficient tandem CD19- and CD22-directed CAR for B cell ALL. Mol. Ther. *30*, 550–563. https://doi.org/10.1016/j.ymthe.2021.08.033.

15. Fry, T.J., Shah, N.N., Orentas, R.J., Stetler-Stevenson, M., Yuan, C.M., Ramakrishna, S., Wolters, P., Martin, S., Delbrook, C., Yates, B., et al. (2018). CD22-CAR T Cells Induce Remissions in CD19-CAR Naïve and Resistant B-ALL. Nat. Med. *24*, 20–28. https://doi.org/10.1038/nm.4441.

16. Singh, N., Frey, N.V., Engels, B., Barrett, D.M., Shestova, O., Ravikumar, P., Cummins, K.D., Lee, Y.G., Pajarillo, R., Chun, I., et al. (2021). Antigen-independent activation enhances the efficacy of 41BB co-stimulated CD22 CAR T cells. Nat. Med. *27*, 842–850. https://doi.org/10.1038/s41591-021-01326-5.

17. Drago, J.Z., Modi, S., and Chandarlapaty, S. (2021). Unlocking the potential of antibody–drug conjugates for cancer therapy. Nat. Rev. Clin. Oncol. *18*, 327–344. https://doi.org/10.1038/s41571-021-00470-8.

18. Fu, Z., Li, S., Han, S., Shi, C., and Zhang, Y. (2022). Antibody drug conjugate: the "biological missile" for targeted cancer therapy. Signal Transduct. Targeted Ther. *7*, 93. https://doi.org/10.1038/s41392-022-00947-7.

19. Stokke, J.L., and Bhojwani, D. (2021). Antibody–drug conjugates for the treatment of acute pediatric leukemia. J. Clin. Med. *10*, 3556. https://doi.org/10.3390/jcm10163556.

20. Ruiz Ciancio, D., Vargas, M.R., Thiel, W.H., Bruno, M.A., Giangrande, P.H., and Mestre, M.B. (2018). Aptamers as Diagnostic Tools in Cancer. Pharmaceuticals *11*, 86. https://doi.org/10.3390/ph11030086.

21. Shigdar, S., Schrand, B., Giangrande, P.H., and de Franciscis, V. (2021). Aptamers: Cutting edge of cancer therapies. Mol. Ther. *29*, 2396–2411. https://doi.org/10.1016/j.ymthe.2021.06.010.

22. Urak, K.T., Blanco, G.N., Shubham, S., Lin, L.H., Dassie, J.P., Thiel, W.H., Chen, Y., Sonkar, V.K., Lei, B., Murthy, S., et al. (2019). RNA inhibitors of nuclear proteins responsible for multiple organ dysfunction syndrome. Nat. Commun. *10*, 116–214. https://doi.org/10.1038/s41467-018-08030-y.

23. Geiger, A., Burgstaller, P., Von der Eltz, H., Roeder, A., and Famulok, M. (1996). RNA aptamers that bind L-arginine with sub-micromolar dissociation constants and high enantioselectivity. Nucleic Acids Res. *24*, 1029–1036. https://doi.org/10.1093/nar/24.6.1029.

24. Chen, L., Rashid, F., Shah, A., Awan, H.M., Wu, M., Liu, A., Wang, J., Zhu, T., Luo, Z., and Shan, G. (2015). The isolation of an RNA aptamer targeting to p53 protein with single amino acid mutation. Proc. Natl. Acad. Sci. USA *112*, 10002–10007. https://doi.org/10.1073/pnas.1502159112.

25. Abeydeera, N.D., Egli, M., Cox, N., Mercier, K., Conde, J.N., Pallan, P.S., Mizurini, D.M., Sierant, M., Hibti, F.E., Hassell, T., et al. (2016). Evoking picomolar binding in RNA by a single phosphorodithioate linkage. Nucleic Acids Res. *44*, 8052–8064. https://doi.org/10.1093/nar/gkw725.

26. Zhou, J., and Rossi, J. (2017). Aptamers as targeted therapeutics: current potential and challenges. Nat. Rev. Drug Discov. *16*, 181–202. https://doi.org/10.1038/nrd.2016.199.

27. Shraim, A.S., Abdel Majeed, B.A., Al-Binni, M.A., and Hunaiti, A. (2022). Therapeutic Potential of Aptamer–Protein Interactions. ACS Pharmacol. Transl. Sci. *5*, 1211–1227. https://doi.org/10.1021/acsptsci.2c00156.

28. Moreno, A., Pitoc, G.A., Ganson, N.J., Layzer, J.M., Hershfield, M.S., Tarantal, A.F., and Sullenger, B.A. (2019). Anti-PEG Antibodies Inhibit the Anticoagulant Activity of PEGylated Aptamers. Cell Chem. Biol. *26*, 634–644.e3. https://doi.org/10.1016/j.chembiol.2019.02.001.

29. Ganson, N.J., Povsic, T.J., Sullenger, B.A., Alexander, J.H., Zelenkofske, S.L., Sailstad, J.M., Rusconi, C.P., and Hershfield, M.S. (2016). Pre-existing anti-polyethylene glycol antibody linked to first-exposure allergic reactions to pegnivacogin, a PEGylated RNA aptamer. J. Allergy Clin. Immunol. *137*, 1610–1613.e7. https://doi.org/10.1016/j.jaci.2015.10.034.

30. Aljohani, M.M., Cialla-May, D., Popp, J., Chinnappan, R., Al-Kattan, K., and Zourob, M. (2022). Aptamers: Potential Diagnostic and Therapeutic Agents for Blood Diseases. Molecules *27*, 383–421. https://doi.org/10.3390/molecules27020383.

31. Camorani, S., Granata, I., Collina, F., Leonetti, F., Cantile, M., Botti, G., Fedele, M., Guarracino, M.R., and Cerchia, L. (2020). Novel Aptamers Selected on Living Cells for Specific Recognition of Triple-Negative Breast Cancer. iScience *23*, 100979. https://doi.org/10.1016/j.isci.2020.100979.

32. Thomas, B.J., Porciani, D., and Burke, D.H. (2022). Cancer immunomodulation using bispecific aptamers. Mol. Ther. Nucleic Acids *27*, 894–915. https://doi.org/10.1016/j.omtn.2022.01.008.

33. Arevalo, A.P., Castelli, R., Ibarra, M., Crispo, M., and Calzada, V. (2022). In Vivo Evaluation of Sgc8-c Aptamer as a Molecular Imaging Probe for Colon Cancer in a Mouse Xenograft Model. Int. J. Mol. Sci. *23*, 1–11. https://doi.org/10.3390/ijms23052466.

34. Porciani, D., Cardwell, L.N., Tawiah, K.D., Alam, K.K., Lange, M.J., Daniels, M.A., and Burke, D.H. (2018). Modular cell-internalizing aptamer nanostructure enables targeted delivery of large functional RNAs in cancer cell lines. Nat. Commun. *9*, 2283. https://doi.org/10.1038/s41467-018-04691-x.

35. Ng, E.W.M., Shima, D.T., Calias, P., Cunningham, E.T., Guyer, D.R., and Adamis, A.P. (2006). Pegaptanib, a targeted anti-VEGF aptamer for ocular vascular disease. Nat. Rev. Drug Discov. *5*, 123–132. https://doi.org/10.1038/nrd1955.

36. Li, Y., Zhao, J., Xue, Z., Tsang, C., Qiao, X., Dong, L., Li, H., Yang, Y., Yu, B., and Gao, Y. (2022). Aptamer nucleotide analog drug conjugates in the targeting therapy of cancers. Front. Cell Dev. Biol. *10*, 1053984. https://doi.org/10.3389/fcell.2022.1053984.

37. Hu, X., Zhang, D., Zeng, Z., Huang, L., Lin, X., and Hong, S. (2022). Aptamer-Based Probes for Cancer Diagnostics and Treatment. Life *12*, 1937. https://doi.org/10.3390/life12111937.

38. Thiel, W.H., Bair, T., Peek, A.S., Liu, X., Dassie, J., Stockdale, K.R., Behlke, M.A., Miller, F.J., and Giangrande, P.H. (2012). Rapid Identification of Cell-Specific, Internalizing RNA Aptamers with Bioinformatics Analyses of a Cell-Based Aptamer Selection. PLoS One *7*, e43836. https://doi.org/10.1371/journal.pone.0043836.

39. Thiel, W.H., Thiel, K.W., Flenker, K.S., Bair, T., Dupuy, A.J., McNamara, J.O., 2nd, Miller, F.J., and Giangrande, P.H. (2015). Cell-Internalization SELEX: Method for Identifying Cell- Internalizing RNA Aptamers for Delivering siRNAs to Target Cells. Methods Mol. Biol. *1218*, 187–199. https://doi.org/10.1007/978-1-4939-1538-5.

40. Tuerk, C., and Gold, L. (1990). Systematic Evolution of Ligands by Exponential Enrichment: RNA Ligands to Bacteriophage T4 DNA Polymerase. Science *249*, 505–510. https://doi.org/10.1126/science.2200121.

41. Ellington, A.D., and Szostak, J.W. (1990). In vitro selection of RNA molecules that bind specific ligands. Nature *346*, 818–822. https://doi.org/10.1038/346818a0.

42. Thiel, W.H., and Giangrande, P.H. (2016). Analyzing HT-SELEX data with the Galaxy Project tools - a web based bioinformatics platform for biomedical research. Methods *97*, 3–10. https://doi.org/10.1146/10.1016/j.ymeth.2015.10.008.

43. Thiel, K.W., Hernandez, L.I., Dassie, J.P., Thiel, W.H., Liu, X., Stockdale, K.R., Rothman, A.M., Hernandez, F.J., McNamara, J.O., 2nd, and Giangrande, P.H. (2012). Delivery of chemo-sensitizing siRNAs to HER2+ -breast cancer cells using RNA aptamers. Nucleic Acids Res. *40*, 6319–6337. https://doi.org/10.1093/nar/gks294.

44. Narayan, C., Veeramani, S., and Thiel, W.H. (2022). Optimization of RNA Aptamer SELEX Methods: Improved Aptamer Transcript 3′-End Homogeneity, PAGE Purification Yield, and Target-Bound Aptamer RNA Recovery. Nucleic Acid Therapeut. *32*, 74–80. https://doi.org/10.1089/nat.2021.0060.

45. Catuogno, S., Di Martino, M.T., Nuzzo, S., Esposito, C.L., Tassone, P., and de Franciscis, V. (2019). An Anti-BCMA RNA Aptamer for miRNA Intracellular Delivery. Mol. Ther. Nucleic Acids *18*, 981–990. https://doi.org/10.1016/j.omtn.2019.10.021.

46. Sicco, E., Baez, J., Ibarra, M., Fernández, M., Cabral, P., Moreno, M., Cerecetto, H., and Calzada, V. (2020). Sgc8-c Aptamer as a Potential Theranostic Agent for Hemato-Oncological Malignancies. Cancer Biother. Radiopharm. *35*, 262–270. https://doi.org/10.1089/cbr.2019.3402.

47. McNamara, J.O., Andrechek, E.R., Wang, Y., Viles, K.D., Rempel, R.E., Gilboa, E., Sullenger, B.A., and Giangrande, P.H. (2006). Cell type-specific delivery of siRNAs with aptamer-siRNA chimeras. Nat. Biotechnol. *24*, 1005–1015. https://doi.org/10.1038/nbt1223.

48. Arber, D.A., Orazi, A., Hasserjian, R., Thiele, J., Borowitz, M.J., Le Beau, M.M., Bloomfield, C.D., Cazzola, M., and Vardiman, J.W. (2016). The 2016 revision to the WHO classification of myeloid neoplasms and acute leukemia. Blood *127*, 2391–2405. https://doi.org/10.1182/blood-2016-03-643544.

49. Schütze, T., Arndt, P.F., Menger, M., Wochner, A., Vingron, M., Erdmann, V.A., Lehrach, H., Kaps, C., and Glökler, J. (2009). A calibrated diversity assay for nucleic acid libraries using DiStRO-a Diversity Standard of Random Oligonucleotides. Nucleic Acids Res. *38*, e23. https://doi.org/10.1093/nar/gkp1108.

50. Thiel, W.H. (2016). Galaxy Workflows for Web-based Bioinformatics Analysis of Aptamer High-throughput Sequencing Data. Mol. Ther. Nucleic Acids *5*, e345. https://doi.org/10.1038/mtna.2016.54.

51. Affinito, A., Quintavalle, C., Esposito, C.L., Roscigno, G., Vilardo, C., Nuzzo, S., Ricci-vitiani, L., De Luca, G., Pallini, R., Kichkailo, A.S., et al. (2019). The Discovery of RNA Aptamers that Selectively Bind Glioblastoma Stem Cells. Mol. Ther. Nucleic Acids *18*, 99–109. https://doi.org/10.1016/j.omtn.2019.08.015.

52. Ferreira, D., Barbosa, J., Sousa, D.A., Silva, C., Melo, L.D.R., Avci-Adali, M., Wendel, H.P., and Rodrigues, L.R. (2021). Selection of aptamers against triple negative breast cancer cells using high throughput sequencing. Sci. Rep. *11*, 8614. https://doi.org/10.1038/s41598-021-87998-y.

53. Walker, J.A., and Smith, K.G.C. (2008). CD22: an inhibitory enigma. Immunology *123*, 314–325. https://doi.org/10.1111/j.1365-2567.2007.02752.x.

54. Ereño-Orbea, J., Liu, X., Sicard, T., Kucharska, I., Li, W., Borovsky, D., Cui, H., Feng, Y., Dimitrov, D.S., and Julien, J.P. (2021). Structural details of monoclonal antibody m971 recognition of the membrane-proximal domain of CD22. J. Biol. Chem. *297*, 100966. https://doi.org/10.1016/j.jbc.2021.100966.

55. Hong, S., Yu, C., Wang, P., Shi, Y., Cao, W., Cheng, B., Chapla, D.G., Ma, Y., Li, J., Rodrigues, E., et al. (2021). Glycoengineering of NK Cells with Glycan Ligands of CD22 and Selectins for B-Cell.pdf. Angew Chem. Int. Ed. Engl. *60*, 3603–3610. https://doi.org/10.1002/anie.202005934.

56. Rico, M.I., Lebedenko, C.G., Mitchell, S.M., and Banerjee, I.A. (2022). Molecular dynamics simulations, docking and MMGBSA studies of newly designed peptide -conjugated glucosyloxy stilbene derivatives with tumor cell receptors. Mol. Divers. *26*, 2717–2743. https://doi.org/10.1007/s11030-021-10354-9.

57. Haso, W., Lee, D.W., Shah, N.N., Stetler-Stevenson, M., Yuan, C.M., Pastan, I.H., Dimitrov, D.S., Morgan, R.A., FitzGerald, D.J., Barrett, D.M., et al. (2013). Anti-CD22–chimeric antigen receptors targeting B-cell precursor acute lymphoblastic leukemia. Blood *121*, 1165–1174. https://doi.org/10.1182/blood-2012-06-438002.

58. Angata, T., Nycholat, C.M., and Macauley, M.S. (2015). Therapeutic Targeting of Siglecs using Antibody- and Glycan- based Approaches. Trends Pharmacol. Sci. *36*, 645–660. https://doi.org/10.1016/j.tips.2015.06.008.

59. Sun, Z., Li, W., Mellors, J.W., Orentas, R., and Dimitrov, D.S. (2022). Construction of a Large Size Human Immunoglobulin Heavy Chain Variable (VH) Domain Library, Isolation and Characterization of Novel Human Antibody VH Domains Targeting PD-L1 and CD22. Front. Immunol. *13*, 869825. https://doi.org/10.3389/fimmu.2022.869825.

60. Chen, D., Oezguen, N., Urvil, P., Ferguson, C., Dann, S.M., and Savidge, T.C. (2016). Regulation of protein-ligand binding affinity by hydrogen bond pairing. Sci. Adv. *2*, e1501240. https://doi.org/10.1126/sciadv.1501240.

61. Masone, D., Vaca, I.C.d., Pons, C., Recio, J.F., and Guallar, V. (2012). H-bond network optimization in protein-protein complexes: Are all-atom force field scores enough? Proteins *80*, 818–824. https://doi.org/10.1002/prot.23239.

62. Ahirwar, R., Nahar, S., Aggarwal, S., Ramachandran, S., Maiti, S., and Nahar, P. (2016). In silico selection of an aptamer to estrogen receptor alpha using computational docking employing estrogen response elements as aptamer-alike molecules. Sci. Rep. *6*, 21285. https://doi.org/10.1038/srep21285.

63. Lee, J., Hitzenberger, M., Rieger, M., Kern, N.R., Zacharias, M., and Im, W. (2020). CHARMM-GUI supports the Amber force fields. J. Chem. Phys. *153*, 035103. https://doi.org/10.1063/5.0012280.

64. Lee, J., Cheng, X., Swails, J.M., Yeom, M.S., Eastman, P.K., Lemkul, J.A., Wei, S., Buckner, J., Jeong, J.C., Qi, Y., et al. (2016). CHARMM-GUI Input Generator for NAMD, GROMACS, AMBER, OpenMM, and CHARMM/OpenMM Simulations Using the CHARMM36 Additive Force Field. J. Chem. Theor. Comput. *12*, 405–413. https://doi.org/10.1021/acs.jctc.5b00935.

65. Jo, S., Kim, T., Iyer, V.G., and Im, W. (2008). CHARMM-GUI: A Web-Based Graphical User Interface for CHARMM. J. Comput. Chem. *29*, 1859–1865. https://doi.org/10.1002/jcc.20945.

66. Humphrey, W., Dalke, A., and Schulten, K. (1996). VMD: Visual Molecular Dynamics. J. Mol. Graph. *14*, 33–38. https://doi.org/10.1016/0263-7855(96)00018-5.

67. Pronk, S., Páll, S., Schulz, R., Larsson, P., Bjelkmar, P., Apostolov, R., Shirts, M.R., Smith, J.C., Kasson, P.M., Van Der Spoel, D., et al. (2013). GROMACS 4.5: A high-throughput and highly parallel open source molecular simulation toolkit. Bioinformatics *29*, 845–854. https://doi.org/10.1093/bioinformatics/btt055.

68. Canoy, R.J., André, F., Shmakova, A., Wiels, J., Lipinski, M., Vassetzky, Y., and Germini, D. (2023). Easy and robust electrotransfection protocol for efficient ectopic

gene expression and genome editing in human B cells. Gene Ther. *30*, 167–171. https://doi.org/10.1038/s41434-020-00194-x.

69. Zhao, N., Qi, J., Zeng, Z., Parekh, P., Chang, C.C., Tung, C.H., and Zu, Y. (2012). Transfecting the hard-to-transfect lymphoma/leukemia cells using a simple cationic polymer nanocomplex. J. Contr. Release *159*, 104–110. https://doi.org/10.1016/j.jconrel.2012.01.007.

70. Fenton, M., Bone, N., and Sinclair, A.J. (1998). The efficient and rapid import of a peptide into primary B and T lymphocytes and a lymphoblastoid cell line. J. Immunol. Methods *212*, 41–48. https://doi.org/10.1016/S0022-1759(97)00208-1.

71. Chen, W.C., Completo, G.C., Sigal, D.S., Crocker, P.R., Saven, A., and Paulson, J.C. (2011). In vivo targeting of B-cell lymphoma with glycan ligands of CD22. Blood *117*, 5551. https://doi.org/10.1182/blood-2011-03-344176.

72. Peng, W., and Paulson, J.C. (2017). CD22 Ligands on a Natural N-Glycan Scaffold Efficiently Deliver Toxins to B-Lymphoma Cells. J. Am. Chem. Soc. *139*, 12450–12458. https://doi.org/10.1021/jacs.7b03208.

73. Harumoto, T., Iwai, H., Tanigawa, M., Kubo, T., Atsumi, T., Tsutsumi, K., Takashima, M., Destito, G., Soloff, R., Tomizuka, K., et al. (2022). Enhancement of Gene Knockdown on CD22-Expressing Cells by Chemically Modified Glycan Ligand-siRNA Conjugates. ACS Chem. Biol. *17*, 292–298. https://doi.org/10.1021/acschembio.1c00652.

74. Tateno, H., Li, H., Schur, M.J., Bovin, N., Crocker, P.R., Wakarchuk, W.W., and Paulson, J.C. (2007). Distinct Endocytic Mechanisms of CD22 (Siglec-2) and Siglec-F Reflect Roles in Cell Signaling and Innate Immunity. Mol. Cell Biol. *27*, 5699–5710. https://doi.org/10.1128/MCB.00383-07.

75. Hu, Y., Li, X., An, Y., Duan, J., and Yang, X.D. (2018). Selection of a novel CD19 aptamer for targeted delivery of doxorubicin to lymphoma cells. Oncotarget *9*, 26605–26615. https://doi.org/10.18632/oncotarget.24902.

76. Esposito, C.L., Van Roosbroeck, K., Santamaria, G., Rotoli, D., Sandomenico, A., Wierda, W.G., Ferrajoli, A., Ruvo, M., Calin, G.A., de Franciscis, V., and Catuogno, S. (2021). Selection of a nuclease-resistant RNA aptamer targeting CD19. Cancers *13*, 5220–5319. https://doi.org/10.3390/cancers13205220.

77. Haghighi, M., Khanahmad, H., and Palizban, A. (2018). Selection and characterization of single-stranded DNA aptamers binding human B-cell surface protein CD20 by cell-SELEX. Molecules *23*, 715. https://doi.org/10.3390/molecules23040715.

78. Shah, N.N., Stevenson, M.S., Yuan, C.M., Richards, K., Delbrook, C., Kreitman, R.J., Pastan, I., and Wayne, A.S. (2015). Characterization of CD22 Expression in Acute Lymphoblastic Leukemia. Pediatr. Blood Cancer *62*, 964–969. https://doi.org/10.1002/pbc.25410.

79. Kantarjian, H.M., DeAngelo, D.J., Stelljes, M., Liedtke, M., Stock, W., Gökbuget, N., O'Brien, S.M., Jabbour, E., Wang, T., Liang White, J., et al. (2019). Inotuzumab ozogamicin versus standard of care in relapsed or refractory acute lymphoblastic leukemia: Final report and long-term survival follow-up from the randomized, phase 3 INO-VATE study. Cancer *125*, 2474–2487. https://doi.org/10.1002/cncr.32116.

80. Bhojwani, D., Sposto, R., Shah, N.N., Rodriguez, V., Yuan, C., Stetler-Stevenson, M., O'Brien, M.M., McNeer, J.L., Quereshi, A., Cabannes, A., et al. (2019). Inotuzumab ozogamicin in pediatric patients with relapsed/refractory acute lymphoblastic leukemia. Leukemia *33*, 884–892. https://doi.org/10.1038/s41375-018-0265-z.

81. Mengxuan, S., Fen, Z., and Runming, J. (2022). Novel Treatments for Pediatric Relapsed or Refractory Acute B-Cell Lineage Lymphoblastic Leukemia: Precision Medicine Era. Front. Pediatr. *10*, 923419. https://doi.org/10.3389/fped.2022.923419.

82. Yang, S., Li, H., Xu, L., Deng, Z., Han, W., Liu, Y., Jiang, W., and Zu, Y. (2018). Oligonucleotide Aptamer-Mediated Precision Therapy of Hematological Malignancies. Mol. Ther. Nucleic Acids *13*, 164–175. https://doi.org/10.1016/j.omtn.2018.08.023.

83. White, R., Rusconi, C., Scardino, E., Wolberg, A., Lawson, J., Hoffman, M., and Sullenger, B. (2001). Generation of species cross-reactive aptamers using "toggle" SELEX. Mol. Ther. *4*, 567–573. https://doi.org/10.1006/mthe.2001.0495.

84. Bitencourt-Ferreira, G., Veit-Acosta, M., and de Azevedo, W.F. (2019). Hydrogen Bonds in Protein-Ligand Complexes. In Docking Screens for Drug Discovery. Methods in Molecular Biology, *2053*, W.F. de Azevedo, ed. (Humana), pp. 93–107. https://doi.org/10.1007/978-1-4939-9752-7_7.

85. Hu, B., Zhou, R., Li, Z., Ouyang, S., Li, Z., Hu, W., Wang, L., and Jiao, B. (2019). Study of the binding mechanism of aptamer to palytoxin by docking and molecular simulation. Sci. Rep. *9*, 15494. https://doi.org/10.1038/s41598-019-52066-z.

86. Su, C.H., Chen, H.L., Ju, S.P., You, T.D., Lin, Y.S., and Tseng, T.F. (2021). Exploring the most stable aptamer/target molecule complex by the stochastic tunnelling-basin hopping-discrete molecular dynamics method. Sci. Rep. *11*, 11406–11416. https://doi.org/10.1038/s41598-021-90907-y.

87. Kandasamy, T., Sudhamalla, B., and Naskar, D. (2022). Designing of RNA aptamer against DNA binding domain of the glucocorticoid receptor: A response element-based in-silico approach. J. Biomol. Struct. Dyn. *40*, 1120–1127. https://doi.org/10.1080/07391102.2020.1822918.

88. Xie, Y.C., Eriksson, L.A., and Zhang, R.B. (2020). Molecular dynamics study of the recognition of ATP by nucleic acid aptamers. Nucleic Acids Res. *48*, 6471–6480. https://doi.org/10.1093/nar/gkaa428.

89. Yoon, S., and Rossi, J.J. (2018). Aptamers: Uptake mechanisms and intracellular applications. Adv. Drug Deliv. Rev. *134*, 22–35. https://doi.org/10.1016/j.addr.2018.07.003.

90. Nuzzo, S., Roscigno, G., Affinito, A., Ingenito, F., Quintavalle, C., and Condorelli, G. (2019). Potential and Challenges of Aptamers as Specific Carriers of Therapeutic Oligonucleotides for Precision Medicine in Cancer. Cancers *11*, 1521–1524. https://doi.org/10.3390/cancers11101521.

91. Liu, Z., Duan, J.H., Song, Y.M., Ma, J., Wang, F.D., Lu, X., and Yang, X.D. (2012). Novel HER2 Aptamer Selectively Delivers Cytotoxic Drug to HER2-positive Breast Cancer Cells in Vitro. J. Transl. Med. *10*, 148. https://doi.org/10.1186/1479-5876-10-148.

92. He, S., Gao, F., Ma, J., Ma, H., Dong, G., and Sheng, C. (2021). Aptamer-PROTAC Conjugates (APCs) for Tumor-Specific Targeting in Breast Cancer. Angew Chem. Int. Ed. Engl. *60*, 23299–23305. https://doi.org/10.1002/anie.202107347.

93. Hernandez, F.J., Stockdale, K.R., Huang, L., Horswill, A.R., Behlke, M.A., and McNamara, J.O. (2012). Degradation of nuclease-stabilized RNA oligonucleotides in Mycoplasma-contaminated cell culture media. Nucleic Acid Therapeut. *22*, 58–68. https://doi.org/10.1089/nat.2011.0316.

94. Veeramani, S., Blackwell, S.E., Thiel, W.H., Yang, Z.Z., Ansell, S.M., Giangrande, P.H., and Weiner, G.J. (2019). An RNA aptamer-based biomarker platform demonstrates high soluble cd25 occupancy by il2 in the serum of follicular lymphoma patients. Cancer Immunol. Res. *7*, 1511–1522. https://doi.org/10.1158/2326-6066.CIR-18-0821.

95. McNamara, J.O., Kolonias, D., Pastor, F., Mittler, R.S., Chen, L., Giangrande, P.H., Sullenger, B., and Gilboa, E. (2008). Multivalent 4-1BB binding aptamers costimulate CD8 + T cells and inhibit tumor growth in mice. J. Clin. Invest. *118*, 376–386. https://doi.org/10.1172/JCI33365.376.

96. Shannon, P., Markiel, A., Ozier, O., Baliga, N.S., Wang, J.T., Ramage, D., Amin, N., Schwikowski, B., and Ideker, T. (2003). Cytoscape: A Software Environment for Integrated Models of Biomolecular Interaction Networks. Genome Res. *13*, 2498–2504. https://doi.org/10.1101/gr.1239303.

97. Chenna, R., Sugawara, H., Koike, T., Lopez, R., Gibson, T.J., Higgins, D.G., and Thompson, J.D. (2003). Multiple sequence alignment with the Clustal series of programs. Nucleic Acids Res. *31*, 3497–3500. https://doi.org/10.1093/nar/gkg500.

98. Will, S., Joshi, T., Hofacker, I.L., Stadler, P.F., and Backofen, R. (2012). Accurate boundary prediction and improved detection of structural RNAs. RNA *18*, 900–914. https://doi.org/10.1261/rna.029041.111.

99. Hofacker, I.L., Fontana, W., Stadler, P.F., Bonhoeffer, L.S., Tacker, M., and Schuster, P. (1994). Fast folding and comparison of RNA secondary structures. Monatsh. Chem. *125*, 167–188. https://doi.org/10.1007/BF00818163.

100. Fontana, W., Konings, D.A., Stadler, P.F., and Schuster, P. (1993). Statistics of RNA secondary structures. Biopolymers *33*, 1389–1404. https://doi.org/10.1002/bip.360330909.

101. Lorenz, R., Bernhart, S.H., Höner, C., Tafer, H., Flamm, C., Stadler, P.F., and Hofacker, I.L. (2011). ViennaRNA Package 2.0. Algorithm Mol. Biol. *6*, 1–14. https://doi.org/10.1186/1748-7188-6-26.

102. Antczak, M., Popenda, M., Zok, T., Sarzynska, J., Ratajczak, T., Tomczyk, K., Adamiak, R.W., and Szachniuk, M. (2016). New functionality of RNAComposer: An application

to shape the axis of miR160 precursor structure. Acta Biochim. Pol. *63*, 737–744. https://doi.org/10.18388/abp.2016_1329.

103. Schneidman-Duhovny, D., Inbar, Y., Nussinov, R., and Wolfson, H.J. (2005). PatchDock and SymmDock: servers for rigid and symmetric docking. Nucleic Acids Res. *33*, 363–367. https://doi.org/10.1093/nar/gki481.

104. Duhovny, D., Nussinov, R., and Wolfson, H.J. (2002). Efficient Unbound Docking of Rigid Molecules. In Algorithms in Bioinformatics. WABI 2002. Lecture Notes in Computer Science, *2452*, R. Guigó and D. Gusfield, eds. (Springer), pp. 185–186. https://doi.org/10.1007/3-540-45784-4_14.

105. Lin, L.H., Taktakishvili, O.M., and Talman, W.T. (2008). Colocalization of neurokinin-1, N-methyl-d-aspartate, and AMPA receptors on neurons of the rat nucleus tractus solitarii. Neuroscience *154*, 690–700. https://doi.org/10.1016/j.neuroscience.2008.03.078.

106. Lin, L.H., Dragon, D.N., Jin, J., and Talman, W.T. (2011). Targeting Neurons of Rat Nucleus Tractus Solitarii with the Gene Transfer Vector Adeno-Associated Virus Type 2 to Up-Regulate Neuronal Nitric Oxide Synthase. Cell. Mol. Neurobiol. *31*, 847–859. https://doi.org/10.1007/s10571-011-9674-5.

107. Lin, L.H., and Talman, W.T. (2006). Vesicular glutamate transporters and neuronal nitric oxide synthase colocalize in aortic depressor afferent neurons. J. Chem. Neuroanat. *32*, 54–64. https://doi.org/10.1016/j.jchemneu.2006.04.004.

108. Lin, L.H., Taktakishvili, O., and Talman, W.T. (2007). Identification and localization of cell types that express endothelial and neuronal nitric oxide synthase in the rat nucleus tractus solitarii. Brain Res. *1171*, 42–51. https://doi.org/10.1016/j.brainres.2007.07.057.

109. Reuter, J.S., and Mathews, D.H. (2010). RNAstructure: Software for RNA secondary structure prediction and analysis. BMC Bioinf. *11*, 129. https://doi.org/10.1186/1471-2105-11-129.